SUPPLEMENTARY MATERIAL

Synthesis of a calcium silicate-carbonate at 122 GPa reveals a missing link in deep-mantle chemistry of silicates and carbonates

*Georgios Aprilis[1], Apostolos Pantousas[1, 2], Alena Aslandukova[3], Ilya Kupenko[1], Xiang Li[1], Susanne Müller[1, 4], Michael Hanfland[1], Leonid Dubrovinsky[2] and *Anna Pakhomova[1]

[1]European Synchrotron Radiation Facility, Grenoble, France
[2]University of Bayreuth, Bayreuth, Germany
[3]Goethe University Frankfurt, Frankfurt am Main, Germany
[4]University of Münster, Münster, Germany

List of contents

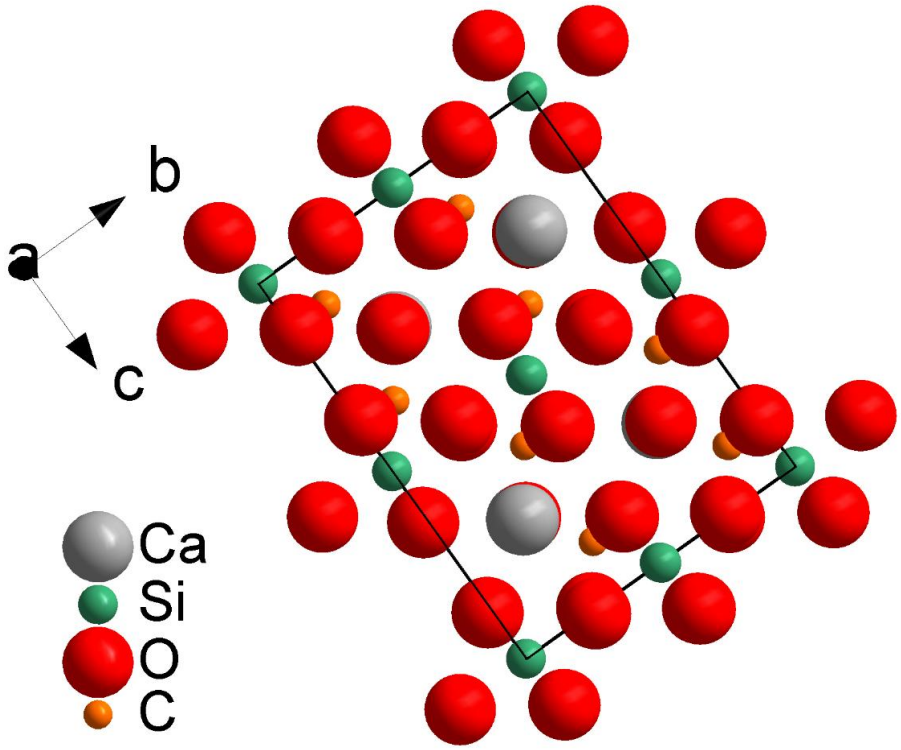

Figure S1. Cubic close packing formed by O and Ca atoms in the crystal structure of $CaSiC_2O_7$ at 122 GPa.

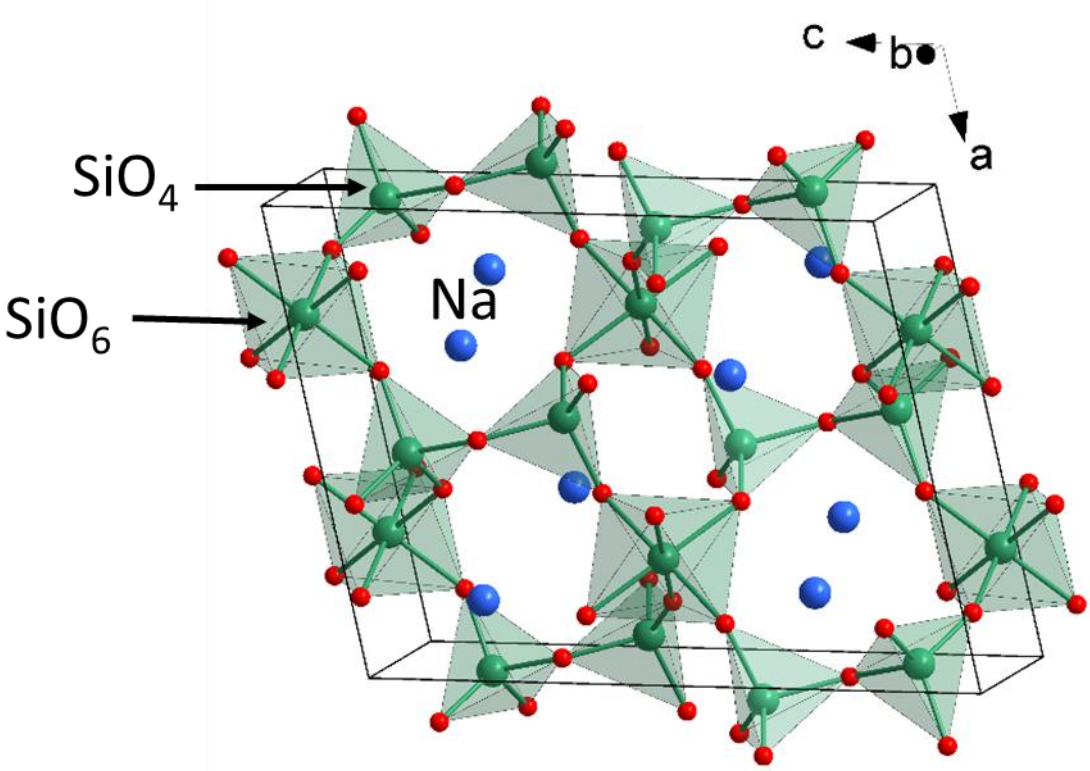

Figure S2. **The crystal structure of sodium trisilicate, $Na_2Si_2C_4O_{14}$, a member of high-pressure framework silicates.** SiO_4 and SiO_6 polyhedra are given in green, Na and O atoms are given as red and blue spheres, respectively. The data is taken from (Fleet and Henderson 1995).

Table S1. Results of the full structural relaxation for $CaSiC_2O_7$ at the experimental unit cell volume.

Pressure (GPa)	Lattice parameters (Å, deg)			Atom	Coordinates		
					x	y	z
127.4	4.469764	6.468101	9.024952	Ca1	0.500000	0.263257	0.250000
	90	90	90	Si1	0.500000	0.000000	0.500000
				C1	0.500000	0.630905	0.379521
				O1	0.500000	0.754399	0.250000
				O2	0.500000	0.747977	0.494805
				O3	0.741130	0.512542	0.369789

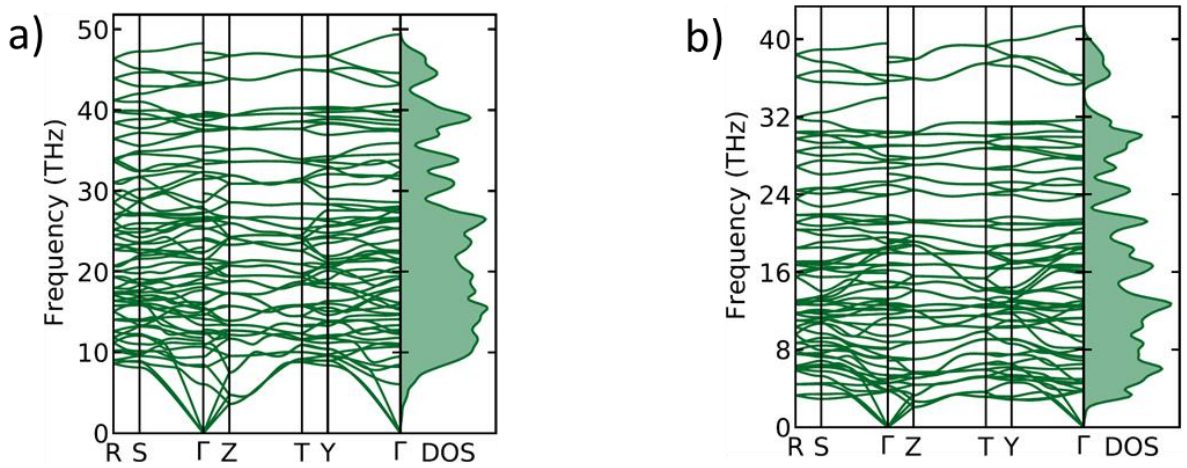

Figure S3. Phonon dispersion curves along high-symmetry directions in the Brillouin zone for $CaSiC_2O_7$ calculated at the experimental volume of ~ 260.91 $Å^3$ (corresponds to theoretical pressure of ~127.4 GPa) (a) and at 1 bar (b).

Table S2. Calculated elastic tensor C_{ij} (in GPa) for $CaSiC_2O_7$ at 122 GPa.

C_{ij}	**1**	**2**	**3**	**4**	**5**	**6**
1	1083.2	406.2	355.4	0	0	0
2	406.2	679.1	481.0	0	0	0
3	355.4	481.0	788.3	0	0	0
4	0	0	0	212.0	0	0
5	0	0	0	0	269.4	0
6	0	0	0	0	0	107.2

Table S3. Calculated elastic tensor C_{ij} (in GPa) for $CaSiC_2O_7$ at 1 bar.

C_{ij}	**1**	**2**	**3**	**4**	**5**	**6**
1	498.0	109.4	72.7	0	0	0
2	109.4	286.3	49.5	0	0	0
3	72.7	49.5	239.8	0	0	0
4	0	0	0	123.6	0	0
5	0	0	0	0	126.2	0
6	0	0	0	0	0	62.1

Text S1. The mechanical stability criteria for an orthorhombic system.

The mechanical stability criteria for an orthorhombic system are (Mouhat and Coudert 2014):

$C_{11} > 0$,

$C_{11}C_{22} > C_{12}^2$,

$C_{11}C_{22}C_{33} + 2C_{12}C_{13}C_{23} - C_{11}C_{23}^2 - C_{22}C_{13}^2 - C_{33}C_{12}^2 > 0$,

$C_{44} > 0$, $C_{55} > 0$, $C_{66} > 0$.

The values of C_{ij} satisfy all of the criteria for mechanical stability for the corresponding pressure points.

Text S2. Calculation of bulk and shear moduli, and compressional and shear wave velocities.

The bulk and shear modulus were derived from elastic constants C_{ij} using following formulas by Voight and Reuss (Reuss 1929):

$$\mathrm{K} = \frac{2 \cdot (C_{11} + C_{12}) + C_{33} + 4 \cdot C_{13}}{9}$$

$$\mathrm{G} = \frac{(2 \cdot C_{11} + C_{13}) - (C_{12} + 2 \cdot C_{13}) + 3 \cdot (2 \cdot C_{44} + \frac{C_{11} - C_{12}}{2})}{5}$$

The compressional Vp and shear Vs wave velocities were calculated from elastic constants C_{ij} according to the following equations:

$$\mathrm{Vp} = \sqrt{\frac{3 \cdot K + 4 \cdot G}{3 \cdot \rho}}$$

$$\mathrm{Vs} = \sqrt{\frac{G}{\rho}}$$

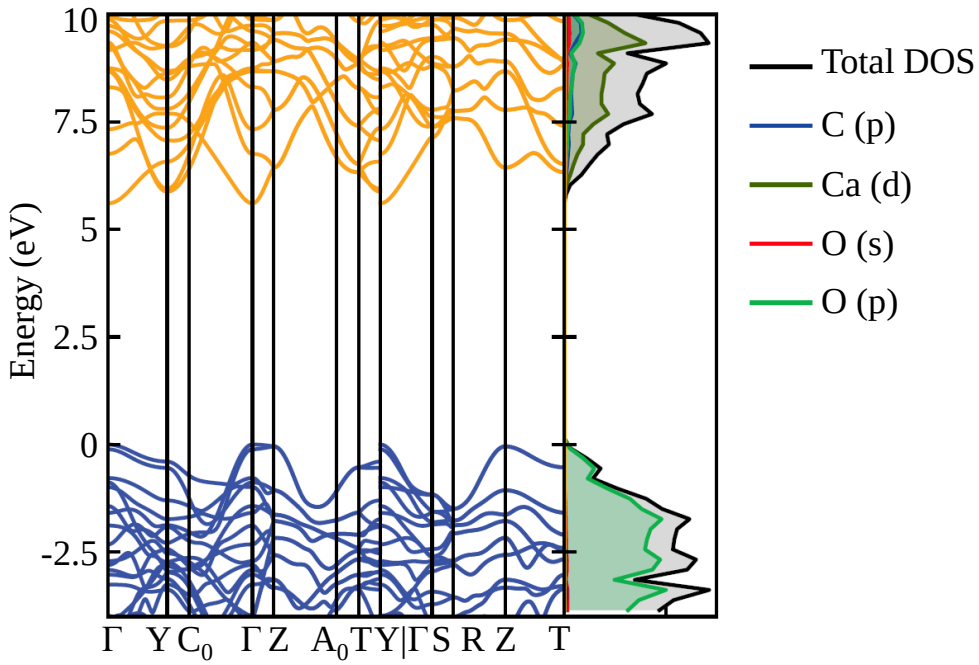

Figure S4. The electronic band structure (left side) and electronic density of states (right side) of $CaSiC_2O_7$ calculated at 122 GPa along high-symmetry directions in the Brillouin zone. The Fermi energy level was set to 0 eV. $CaSiC_2O_7$ is a wide-bandgap semiconductor with a direct band gap of 5.606 eV.

Table S4. Overview of the previous high-pressure-high-temperature experiments on the (Ca,Mg,Fe)-Si-C-O system. Temperatures are rounded to the 100s.

P (GPa)	T(K)	Reactants	Observed new phases	References
28 – 123	1600 – 3200	$CaCO_3$ + Fe_3Si	$CaSiO_3$ + Fe_3C + Fe_7C_3 + FeO + CaO + SiO_2	(Davis et al. 2024)
33 – 77	2200 – 3000	$MgCO_3$ + Fe_3Si	$MgSiO_3$ + Fe_3C + Fe_7C_3 + MgO + FeO + SiO_2	
< 80	< 2300	MORB glass + $CaCO_3$ (calcite) $MgSiO_3$ (Mg-perovskite) + $CaCO_3$ (aragonite)	$CaSiO_3$ (Ca-perovskite) + $MgCO_3$ (magnesite)	(Seto et al. 2008)
60 – 80	> 2400	$MgCO_3$ (magnesite) + SiO_2 (stishovite)	$MgSiO_3$ (Mg-perovskite) + C (diamond) + O_2 (ε-oxygen)	
33 – 83	1600 – 2500	$(Mg,Ca)CO_3$ + $(Mg,Fe)SiO_3$	$MgCO_3$ + $CaSiO_3$	(Lv et al. 2021)
88 – 137	2000 – 2800	$(Mg,Ca)CO_3$ + $(Mg,Fe)SiO_3$	$CaCO_3$ + $MgSiO_3$	
50 – 88	1600 – 1900	$(Mg,Fe)CO_3$ + SiO_2	$(Mg,Fe)SiO_3$ + CO_2 / (C + O_2)	(Drewitt et al. 2019)
46 – 89	1600 – 1900	$CaMg(CO_3)_2$ + SiO_2	$MgSiO_3$ + $CaSiO_3$ + CO_2 / (C + O_2)	
20 - 50	1500 – 2500	$(Mg_{0.88}, Fe_{0.12})SiO_3$ (enstatite) + $CaMg(CO_3)_2$ (dolomite)	$CaSiO_3$ (Ca-perovskite) + $2{\cdot}Mg_{0.94}Fe_{0.06}CO_3$ (magnesite) + cubic majoritic garnet	(Biellmann et al. 1993)
40	1500 – 2500	$(Mg_{0.88}, Fe_{0.12})SiO_4$ (olivine) + $CaMg(CO_3)_2$ (dolomite)	$CaSiO_3$ (Ca-perovskite) + $2{\cdot}Mg_{1-x}Fe_xCO_3$ (magnesite) + $(Mg_{1-y},Fe_y)O$ (magnesiowüstite)	
51 – 113	1800 – 2500	$(Mg_{0.38}Ca_{0.59}Fe_{0.03})CO_3$ (dolomite) + Fe	Fe_7C_3 + FeO + MgO + $CaCO_3$ + C	(Dorfman et al. 2018)

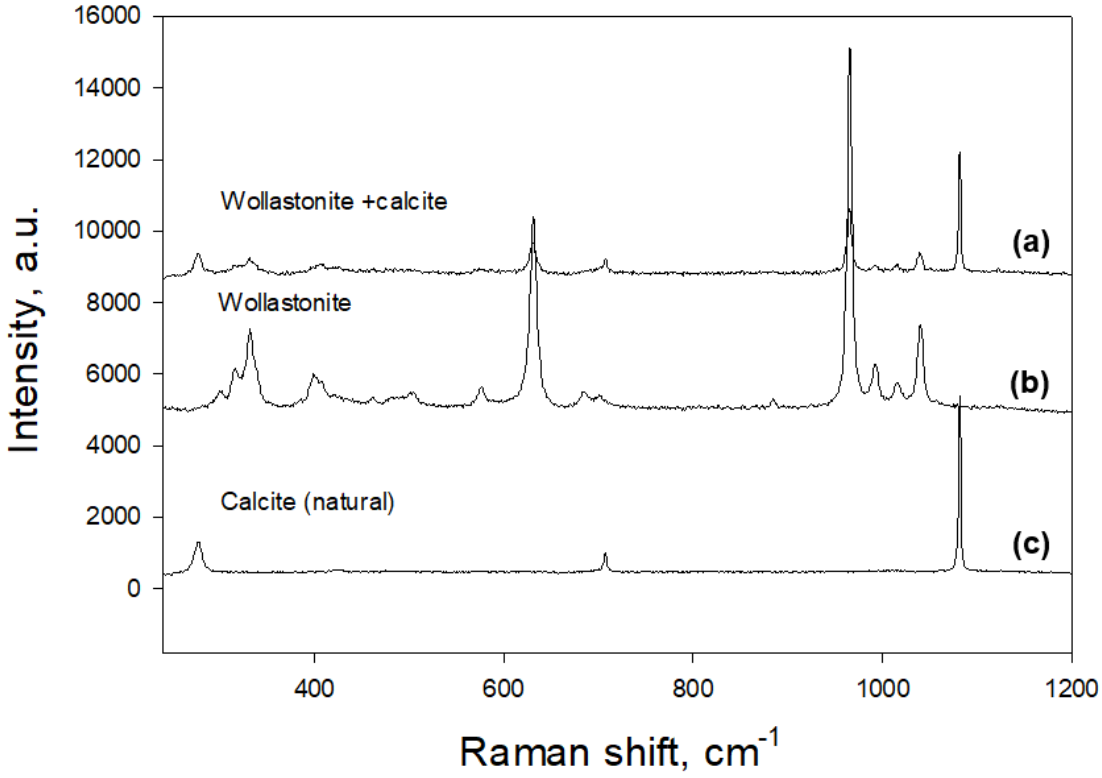

Figure S5. Raman spectra of the starting material at ambient conditions: (a) natural wollastonite with the presence of calcite; (b) natural wollastonite without calcite from a different location on the sample; (c) natural calcite used as reference. It was not possible to locate the calcite crystals physically, probably due to their small size. The spectra were collected using a LabRam system equipped with a He-Ne laser (632 nm) and a x50 Mitutoyo objective at the Bayerisches Geoinstitut. The collection time was 2 x 100 s for each spectrum.

References

Biellmann, C., Gillet, P., Guyot, F., Peyronneau, J., and Reynard, B. (1993) Experimental evidence for carbonate stability in the Earth's lower mantle. Earth and Planetary Science Letters, 118, 31–41.

Davis, A.H., Chidester, B.A., Greenberg, E., Prakapenka, V.B., and Campbell, A.J. (2024) Carbonate-Metal Reactions in the Lower Mantle. ACS Earth and Space Chemistry, 8, 654–664.

Dorfman, S.M., Badro, J., Nabiei, F., Prakapenka, V.B., Cantoni, M., and Gillet, P. (2018) Carbonate stability in the reduced lower mantle. Earth and Planetary Science Letters, 489, 84–91.

Drewitt, J.W.E., Walter, M.J., Zhang, H., McMahon, S.C., Edwards, D., Heinen, B.J., Lord, O.T., Anzellini, S., and Kleppe, A.K. (2019) The fate of carbonate in oceanic crust subducted into earth's lower mantle. Earth and Planetary Science Letters, 511, 213–222.

Fleet, M.E., and Henderson, G.S. (1995) Sodium trisilicate: A new high-pressure silicate structure (Na2Si[Si2O7]). Physics and Chemistry of Minerals, 22, 383–386.

Lv, M., Dorfman, S.M., Badro, J., Borensztajn, S., Greenberg, E., and Prakapenka, V.B. (2021) Reversal of carbonate-silicate cation exchange in cold slabs in Earth's lower mantle. Nature Communications, 12, 1712.

Mouhat, F., and Coudert, F.-X. (2014) Necessary and sufficient elastic stability conditions in various crystal systems. Physical Review B, 90, 224104.

Reuss, A. (1929) Berechnung der Fließgrenze von Mischkristallen auf Grund der Plastizitätsbedingung für Einkristalle . ZAMM - Journal of Applied Mathematics and Mechanics / Zeitschrift für Angewandte Mathematik und Mechanik, 9, 49–58.

Seto, Y., Hamane, D., Nagai, T., and Fujino, K. (2008) Fate of carbonates within oceanic plates subducted to the lower mantle, and a possible mechanism of diamond formation. Physics and Chemistry of Minerals, 35, 223–229.